Int. J. Electrochem. Sci., 17 **(2022)** Article Number: 220754, doi: 10.20964/2022.07.41

International Journal of
ELECTROCHEMICAL
SCIENCE
www.electrochemsci.org

A Novel State of Health Estimation of Lithium-ion Battery Energy Storage System Based on Linear Decreasing Weight-Particle Swarm Optimization Algorithm and Incremental Capacity-Differential Voltage Method

Zhuoyan Wu[1], Likun Yin[1], Ran Xiong[2,3,], Shunli Wang[3], Wei Xiao[2], Yi Liu[2], Jun Jia[2], Yanchao Liu[1]*

[1] Science and Technology Research Institute, China Three Gorges Corporation, Beijing, 100038, China;
[2] Sichuan Energy Internet Research Institute, Tsinghua University, Chengdu, 610042, China;
[3] School of Information Engineering, Southwest University of Science and Technology, Mianyang 621010, China.
[*]E-mail: 438394119@qq.com

Received: 1 April 2022 / *Accepted:* 6 May 2022 / *Published:* 6 June 2022

Accurate estimation of battery state of health (SOH) under energy storage conditions is a key and difficult technology in the use of lithium-ion batteries, which is related to the health and safety of batteries, use efficiency, and product replacement. Because of the complex working conditions of energy storage batteries, it is necessary to use a method to estimate SOH, which takes into account both the internal electrochemical mechanism and the battery degradation mechanism. Based on this requirement, a SOH estimation method for energy storage lithium-ion batteries based on linear decreasing weight-particle swarm optimization (LDW-PSO) algorithm and incremental capacity-differential voltage (IC-DV) method is proposed. The algorithm uses the LDW-PSO method to identify the maximum solid-phase lithium-ion concentration of positive and negative electrodes in the single particle (SP) model, quantifies degradation modes by the IC-DV method, and takes the above parameters as the input of the back propagation neural network (BPNN) to estimate the SOH of energy storage lithium-ion batteries. At 25 ℃, the working condition of an actual energy storage power station is used for simulation and verification. The experimental results show that the maximum estimation error, the mean estimation error, and the mean square error (MSE) of the battery SOH in test data are 0.0474%, 0.0261%, and 8.87×10^{-8}, respectively, and the maximum estimation error, the mean estimation error, and the MSE of the battery SOH in the same batch with the same degradation path are 0.0077, 0.0012, and 5.24×10^{-6}, respectively. The above results provide a theoretical and experimental basis for the problem that the SOH of lithium-ion batteries cannot be effectively estimated under complex working conditions of energy storage power stations.

Keywords: electrochemical and degradation mechanisms; state of health; single particle model; linear decreasing weight-particle swarm optimization algorithm; incremental capacity-differential voltage method; back propagation neural network

1. INTRODUCTION

Electrochemical energy storage technology has been widely used in grid-scale energy storage to promote the absorption of renewable energy and peak modulation[1, 2]. Energy storage system has been concerned by the field of clean energy research, and the design methods of related materials continue to appear in a large number of studies[3]. Energy storage lithium battery is the core equipment of energy storage power stations, and it is the key to realize the functions of load compensation, peak cutting and valley filling in energy storage power station. Its safety performance is of great significance to the stable and reliable operation of energy storage power station.

With the degradation of lithium battery, the internal resistance of lithium battery increases, the risk of thermal runaway increases, and the possibility of explosion increases, such as an energy storage power station accident in South Korea in 2018[4] and a delayed explosion in 2019[5]. Sound battery management is a prerequisite for ensuring the safe and stable operation of lithium-ion batteries[6, 7]. The battery management system can monitor the states such as SOH to ensure that the battery is in the safe working range[8-11]. Therefore, it is necessary to estimate the changes of lithium battery SOH in the degradation cycles, so as to provide a basis for the next development of operation and maintenance plan. SOH is one of the most important states in battery operation, which is usually defined by the ratio of available capacity to rated capacity[12-14]. Compared with the new battery, the SOH reflects the ability of the battery to provide the required performance[15]. Accurate SOH estimation of energy storage battery can extend the life of energy storage system and improve safety.

At present, the algorithms for estimating battery SOH at home and abroad can be mainly divided into direct measurement method, data-driven method, physical model-based method and hybrid model-based method. The direct measurement method is the easiest method because it uses a complete discharge cycle to calculate the available capacity of the battery[15]. However, this method is not practical in application, because it is difficult to measure the battery state directly with the instrument, so it is more reasonable to estimate SOH by relevant parameters[16].

Instead of building specific physics-based models, data-driven methods use a class of statistical theories or machine learning techniques to derive mathematical prediction models directly from measured data. SOH estimation with data-driven method can omit some physical modeling steps, so it has strong adaptability and applicability, which has attracted wide attention of researchers at home and abroad. However, the data-driven estimation method requires a lot of experimental data and the training process is complex.

In recent years, the common data-driven estimation methods in the literature include support vector machine (SVM), correlation vector machine (CVM), Gaussian process regression (GPR), neural network (NN), fuzzy logic (FL), deep learning (DL) and so on[17-20]. For example, Che estimated the SOH of the battery through a nonlinear autoregressive neural network model based on exogenous input, and verified the accuracy of the algorithm in single-cell and multi-cell experiments[21]. In [22], Gong

proposed an encoder-decoder model based on deep learning to estimate SOH. The encoder is a hybrid neural network, which can effectively encode the sampling data of the charging curve and generate a coding sequence. The decoder is mainly composed of BPNN, which is responsible for decoding the coding sequence to output the estimated value of SOH. The experimental results show that this method has high estimation accuracy for different types of batteries. Xiong extracted some features from the battery charging curve as input to the estimation model and estimated battery SOH based on the weighted least squares-support vector machine (WLS-SVM). The accuracy of the algorithm was verified under different degradation paths and degradation degrees[23]. However, due to the limited ability of the above-mentioned data-driven methods to characterize battery characteristics offline, some scholars have proposed data-driven analysis methods such as the incremental capacity (IC) method, which have relatively eclectic effects when estimating battery states offline and online[24]. Nevertheless, the implementation of this kind of method still needs a large amount of experimental data, and the error will increase exponentially if there is an error.

Therefore, the method based on physical model is proposed to be suitable for scenarios with less experimental data. The premise of using the physical model-based method to estimate the battery state is to establish a suitable battery physical model. At present, the single physical models for estimating the SOH of lithium-ion batteries include equivalent circuit model (ECM) and electrochemical model (EM).

ECMs simulate the dynamic voltage characteristics of the battery based on circuit elements such as power sources, inductors, capacitors, and resistors. The common ECMs include Rint model, Thevenin model, second-order RC model, PNGV model and GNL model. The ECM often estimates SOH by combining filtering methods. For example, reference document [25] studied a dual adaptive extended Kalman filter algorithm based on second-order ECM to jointly estimate SOC and SOH, and verified the accuracy and robustness of this algorithm at 25 ℃. Qiao utilized a bias compensation recursive least square-multiple weighted dual extended Kalman filtering method based on second-order ECM to jointly estimate SOC and SOH. This method introduces bias compensation to adjust system noise parameters and reduce the influence of system colored noise[26]. Zeng improved the second-order ECM, and used the fuzzy unscented Kalman algorithm to jointly estimate battery SOC and SOH on this basis[27]. Ling [28] estimated battery SOC and SOH based on a dual fractional-order extended Kalman filter algorithm, and verified the accuracy and applicability of the algorithm under three working conditions.

Based on porous electrode theory and concentrated solution theory, the EM describes batteries from the perspective of electrochemical mechanism. Therefore, the EM can reflect the battery performance more realistically, which leads to the high accuracy but the complex calculation of the model. At present, the common EMs used to estimate battery states include pseudo-two-dimensional (P2D) model, single particle (SP) model and other simplified P2D models. The P2D model is an electrochemical model proposed by Doyle, which is usually regarded as the baseline mechanism model in the electrochemical models[29]. However, the P2D model contains a large number of nonlinear equations, which leads to the unsatisfactory calculation efficiency. The SP model is the most simplified P2D model and it only has good performance in low-rate charge and discharge[30]. Under high-rate conditions, it may lead to excessive deviation of the results. For example, Mehta investigated an improved SP model to estimate battery state without increasing any significant computational complexity[31]. This model takes into account the spatial variation of overpotential and open-circuit

potential. In reference [32], Deng used the polynomial approximation principle for reducing the P2D model to form a simplified model to estimate the battery state.

Data-driven methods for estimating battery state do not rely on physical models, which may lead to large errors in results. The state estimation method based on the ECM is simple in calculation but low in accuracy. The state estimation method based on the EM has high accuracy but complex calculation. Therefore, in recent years, some scholars have proposed a series of state estimation methods based on hybrid models. For example, Esfandyari put forward a method for estimating the SOH and SOP of a series-connected lithium-ion battery pack for hybrid electric vehicles based on model prediction and fuzzy logic, which uses a model that combines ECM and data-driven[33]. In addition, Park also analyzed a hybrid model combining ECM and data-driven methods for estimating battery SOH[34]. The model combines the Thevenin ECM and the multivariate autoregressive algorithm, and is used for real-time estimation and prediction of capacity when the amount of measured data is insufficient. In [35], Chu proposed a hybrid model combining electrochemical mechanism and data-driven. This method utilizes the Nyquist impedance diagram to propose an ECM based on characterizing the electrochemical reaction process for battery state estimation. This kind of hybrid model of EM-ECM takes into account both the external and internal electrochemical characteristics of the battery, but the theoretical basis and practical basis are few, and the calculation is difficult.

In this paper, the maximum solid-phase lithium-ion concentration of positive and negative electrodes in SP model is identified by the LDW-PSO method, and the battery degradation modes are quantified by the IC-DV method. On the basis of taking the maximum solid-phase lithium-ion concentration of positive and negative electrodes and degradation modes as the input of BPNN, a novel SOH estimation method of energy storage lithium-ion batteries based on the LDW-PSO algorithm and the IC-DV method is proposed. The algorithm considers the electrochemical mechanism of the battery, and studies the variation of the solid-phase lithium-ion concentration from the microscopic level. In order to solve the problem that the PSO algorithm may fall into local optimization, the identification algorithm proposed in this paper introduces the weight factor on the basis of the PSO algorithm. Besides, in order to explore the influence of the degradation mechanism on the battery SOH, the algorithm proposed in this paper uses the IC-DV method to quantify the degradation modes, which can lay a foundation for subsequent estimation of SOH. The simulation results show that the BPNN model proposed in this paper improves the interpretability and accuracy of SOH estimation results compared with the model using voltage and current as input to BPNN.

The rest of this paper is organized as follows: Section 2 introduces the mathematical analysis, including SP modeling, LDW-PSO parameter identification, quantification method of degradation modes based on IC-DV, grey relational analysis and BPNN. Among them, grey relational analysis method is used to analyze the relational degree between input and output of BPNN in this paper. Details of the experimental results are described in section 3. And finally, section 4 presents the main conclusions of the full text.

2. MATHEMATICAL ANALYSIS

2.1. Single particle modeling

In order to accurately identify the maximum solid-phase lithium-ion concentration of positive and negative electrodes to estimate the SOH of lithium-ion batteries, it is an important process to select a suitable battery electrochemical model. Since the battery in this paper is tested under the low-rate condition, the SP model can accurately characterize the internal electrochemical characteristics of lithium-ion batteries and meet the requirements of some engineering applications. The SP model is a simplified electrochemical model of lithium-ion battery based on the characteristics of a spherical particle in the electrode to represent the characteristics of the whole electrode[36].

The SP model has a simple structure and few parameters. Compared with the Rint model, the simulation time of the SP model is similar to that of the Rint model, and the SP model has higher accuracy in battery performance prediction and state estimation. Compared with P2D model, the accuracy of SP model is lower, but the simulation speed is faster[37]. Therefore, the SP model is selected based on the above analysis, which is shown in Figure 1.

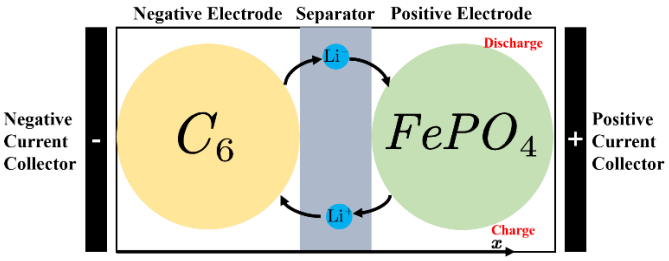

Figure 1. The SP model of the energy storage lithium battery

Figure 1 is a schematic diagram of the SP model of lithium iron phosphate battery. The conditions for establishing the single particle model include:

(1) It is assumed that the electrode of lithium-ion battery is composed of several spherical particles with the same size and dynamic characteristics, and the current is uniformly distributed among all active particles as it passes through the electrode;

(2) It is assumed that the voltage drop within or between solid particles is zero;

(3) It is assumed that the liquid-phase lithium-ion concentration is constant in the whole battery and uniformly distributed in time and space;

(4) The effect of liquid-phase voltage on battery terminal voltage is ignored;

(5) The effect of heat generated during charge and discharge on battery electrochemical reaction is ignored.

Therefore, only the basic working process, solid-phase diffusion, reaction polarization and ohmic polarization are included in the SP model. Based on the above assumptions, it is known that the molar reaction flux density is also equal in an electrode. The expression of the molar reaction flux density at the boundary of the positive and negative electrode collectors is shown in the following formula.

$$j_i = \frac{IR_{s,i}}{3F\left(1-\varepsilon_i-\varepsilon_{f,i}\right)l_i A_i}, i = p,n \tag{1}$$

In Equation (1), $R_{s,i}$ stands for the radius of the particle, F represents Faraday constant, ε_i represents the material porosity, $\varepsilon_{f,i}$ represents the filling substance volume fraction, l_i is the plate thickness, and A_i is the effective area of pole piece. Besides, i is used to distinguish the polarity of the battery. p represents the positive electrode, and n represents the negative electrode.

According to the internal physical characteristics of the battery, the terminal voltage of the battery is the difference between the positive solid-phase potential and the negative solid-phase potential. Since the SP model ignores the liquid-phase diffusion process, the liquid-phase potential at each position in the electrode is zero. Combining solid-phase diffusion process, reaction polarization process and ohmic polarization process, the expression of the terminal voltage of the lithium-ion battery is shown below.

$$U_t = \Phi_{s,p} - \Phi_{s,n} = E_p\left(\frac{c_{s,surf,p}}{c_{s,\max,p}}\right) + \eta_{act,p} + \eta_{ohm,p} - \left(E_n\left(\frac{c_{s,surf,n}}{c_{s,\max,n}}\right) + \eta_{act,n} + \eta_{ohm,n}\right) = E + \eta_{act} + \eta_{ohm} \tag{2}$$

In Equation (2), U_t represents the terminal voltage, $\Phi_{s,p}$ represents the positive solid-phase potential, $\Phi_{s,n}$ represents the negative solid-phase potential, E_p represents the positive open potential, E_n represents the negative open potential, $c_{s,surf,p}$ represents the solid-phase Li-ion concentration on the surface of the positive electrode, $c_{s,surf,n}$ represents the solid-phase Li-ion concentration on the surface of the negative electrode, $c_{s,max,p}$ represents the maximum solid-phase Li-ion concentration of the positive electrode, $c_{s,max,n}$ represents the maximum solid-phase Li-ion concentration of the negative electrode, $\eta_{ohm,p}$ is the ohmic polarization potential of positive electrode, $\eta_{ohm,n}$ is the ohmic polarization potential of negative electrode, η_{act} stands for the reaction polarization overpotential, η_{ohm} stands for the ohmic polarization overpotential, and E is the open potential. Among them, E can be calculated by the following formula.

$$E = E_p\left(\frac{c_{s,surf,p}}{c_{s,\max,p}}\right) - E_n\left(\frac{c_{s,surf,n}}{c_{s,\max,n}}\right) \tag{3}$$

It can be seen from Equation (3) that E is related to $c_{s,surf,i}$ and $c_{s,max,i}$ (i=p,n). $c_{s,surf,i}$ can be obtained by the three-parameter parabolic equation of solid-phase diffusion. The solid-phase diffusion process of lithium-ion obeys Fick's second law. The diffusion equation of lithium-ion in solid particles can be established by using spherical coordinate system. The governing equation of the solid-state diffusion is shown as follows.

$$\frac{\partial c_{s,i}}{\partial t} = D_{s,i}\frac{1}{r^2}\frac{\partial}{\partial r}\left(r^2\frac{\partial c_{s,i}}{\partial r}\right), i = p,n \tag{4}$$

In Equation (4), $c_{s,i}$ represents the solid-phase Li-ion concentration, $D_{s,i}$ represents the solid-phase Li-ion diffusion coefficient and r represents the radial distance coordinate of the particle. The boundary and initial conditions in Equation (4) are shown in Equation (5).

$$\begin{cases} \left.\dfrac{\partial c_{s,i}}{\partial r}\right|_{r=0} = 0 \\ \left.\dfrac{\partial c_{s,i}}{\partial r}\right|_{r=R_i} = -\dfrac{j_i}{D_{s,i}} \end{cases}, i = p,n \tag{5}$$

In Equation (5), j_i represents the molar reaction flux density at the boundary of the positive and

negative collector, and $R_{s,i}$ represents the radius of the particle. Equation (4) is a parabolic partial differential equation. According to the definition of the parabolic partial differential equation, the solid-phase concentration distribution along the particle radius direction is parabolic at any time. Therefore, the parabolic approximation model can be used to simplify the solid-phase concentration diffusion equation to obtain the particle solid-phase surface concentration. In order to balance the computational complexity and the simulation accuracy, the three-parameter parabola method is used to simplify the solution of Equation (4). The distribution expression of spherical particle solid-phase lithium-ion concentration along the radial direction is shown in Equation (6).

$$c_{s,i}(t,r) = a(t) + b(t)\left(\frac{r^2}{R_{s,i}^2}\right) + c(t)\left(\frac{r^4}{R_{s,i}^4}\right), i = p,n \tag{6}$$

In Equation (6), $a(t)$, $b(t)$ and $c(t)$ are the coefficients that need to be solved. Two equations about $a(t)$, $b(t)$ and $c(t)$ can be obtained by bringing Equation (6) into Equation (4) and Equation (5), as shown in the following formulas.

$$\begin{cases} \dfrac{da(t)}{dt} = \dfrac{r^2}{R_{s,i}^2}\dfrac{db(t)}{dt} + \dfrac{r^4}{R_{s,i}^4}\dfrac{dc(t)}{dt} = \dfrac{2D_{s,i}}{R_{s,i}^2}\left(3b(t) + 10\dfrac{r^2}{R_{s,i}^2}c(t)\right) \\ \dfrac{2D_{s,i}}{R_{s,i}^2}b(t) + \dfrac{4D_{s,i}}{R_{s,i}}c(t) + j_i = 0 \end{cases}, i = p,n \tag{7}$$

For the solid-phase diffusion process in active particles, the key variables are the average solid-phase lithium-ion concentration, the solid-phase surface lithium-ion concentration and the average particle concentration flux. At the same time, because Equation (7) contains three unknowns, the above three variables are introduced to solve the equations. The specific expression is shown in the following formulas.

$$\begin{cases} q_{s,avg,i}(t) = \int_{r=0}^{R_{s,i}} 3\dfrac{r^2}{R_{s,i}^2}\left(\dfrac{\partial}{\partial r}c_{s,i}(t,r)\right)d\left(\dfrac{r}{R_{s,i}}\right) = \dfrac{2b(t)}{3R_{s,i}} + 2\dfrac{c(t)}{R_{s,i}} \\ c_{s,surf,i}(t) = a(t) + b(t) + c(t) \\ c_{s,avg,i}(t) = \int_{r=0}^{R_{s,i}} 3\dfrac{r^2}{R_{s,i}^2}c_{s,i}(t,r)d\left(\dfrac{r}{R_{s,i}}\right) = a(t) + \dfrac{3}{5}b(t) + \dfrac{3}{7}c(t) \end{cases}, i = p,n \tag{8}$$

In Equation (8), $q_{s,\,avg,i}$ represents the average particle concentration flux, $c_{s,\,surf,i}$ represents the solid-phase surface lithium-ion concentration, and $c_{s,avg,i}$ represents average solid-phase lithium-ion concentration. The expressions of $a(t)$, $b(t)$ and $c(t)$ can be obtained by changing Equation (8), as shown below.

$$\begin{cases} a(t) = \dfrac{39}{4}c_{s,surf,i}(t) - 3q_{s,avg,i}(t)R_{s,i} - \dfrac{35}{4}c_{s,avg,i}(t) \\ b(t) = -35c_{s,surf,i}(t) + 10q_{s,avg,i}(t)R_{s,i} + 35c_{s,avg,i}(t) \\ c(t) = \dfrac{105}{4}c_{s,surf,i}(t) - 7q_{s,avg,i}(t)R_{s,i} - \dfrac{105}{4}c_{s,avg,i}(t) \end{cases}, i = p,n \tag{9}$$

By substituting the expressions of $a(t)$, $b(t)$ and $c(t)$ in Equation (9) into Equation (7), the expression of the lithium-ion concentration on the solid-phase surface can be obtained, which is shown in the following formulas.

$$\begin{cases} c_{s,avg,i}(t) = c_{s,0,i} - \int_0^t 3\frac{j_i}{R_{s,i}}dt \\ \frac{d}{dt}q_{s,avg,i}(t) + 30\frac{D_{s,i}}{R_{s,i}^{\ 2}}q_{s,avg,i}(t) + \frac{45j_i}{2R_{s,i}^{\ 2}} = 0 \qquad ,i = n, p \\ c_{s,surf,i}(t) = c_{s,avg,i}(t) + \left(8D_{s,i}q_{s,avg,i}(t) - j_i\right)\frac{R_{s,i}}{35D_{s,i}} \end{cases} \tag{10}$$

In Equation (10), $c_{s,0,i}$ represents the initial solid-phase Li-ion concentration. The known boundary conditions are shown in the following formulas.

$$\begin{cases} q_{s,avg,i}(t)\big|_{t=0} = 0 \\ c_{s,surf,i}\big|_{t=0} = c_{s,surf,0,i} \end{cases} \tag{11}$$

In Equation (11), $c_{s,surf,0,i}$ represents the initial surface Li-ion concentration of solid-phase particle. The lithium-ion concentration curve on the solid-phase surface of positive and negative electrodes can be obtained by combining Equation (10) and Equation (11), and then the open circuit potential can be obtained by Equation (3). In Equation (3), η_{act} represents the reaction polarization overpotential, and it provides the power to maintain the corresponding electrochemical reaction rate. η_{act} can be calculated as follows.

$$\eta_{act} = \eta_{act,p} - \eta_{act,n} \tag{12}$$

In Equation (12), $\eta_{act,p}$ and $\eta_{act,n}$ represent the reaction polarization overpotential of positive electrode and the reaction polarization overpotential of negative electrode, respectively. Lithium ions diffuse between the solid-phase and the electrolyte interface. The Butler-Volmer kinetic equation describes the electrochemical reaction process at the solid-liquid phase interface in the positive and negative electrodes of lithium batteries. During the reaction process, the relationship between the reaction polarization overpotential and the lithium-ion concentration can be expressed by the Butler-Volmer equation, as shown in the following formula.

$$j_i = k_i\left(c_{s,\max,i} - c_{s,surf,i}(t)\right)^{0.5}\left(c_{s,surf,i}(t)\right)^{0.5}c_e^{\ 0.5}\left(\exp\left(\frac{0.5F}{RT}\right)\eta_{act,i} - \exp\left(-\frac{0.5F}{RT}\right)\eta_{act,i}\right) \tag{13}$$

Wherein, k_i represents the average electrode reaction rate constant, c_e represents the liquid Li-ion concentration, R represents the universal gas constant, T is the battery temperature. According to Equation (13), the positive and negative reaction polarization overpotential expressions can be obtained, as shown below.

$$\begin{cases} \eta_{act,i} = \frac{2RT}{F}\ln\left(m_i + \sqrt{m_i^{\ 2} + 1}\right) \\ m_i = \frac{j_i}{2k_i\left(c_{s,\max,i} - c_{s,surf,i}(t)\right)^{0.5}\left(c_{s,surf,i}(t)\right)^{0.5}c_e^{\ 0.5}} \end{cases} \tag{14}$$

In the SP model, it is considered that the ohmic polarization overpotential of the battery is mainly due to the ohmic polarization overpotential of SEI film. The expression for calculating the ohmic polarization overpotential is shown in the following formula.

$$\eta_{ohm} = \eta_{ohm,p} - \eta_{ohm,n} = R_{SEI,p}Fj_p - R_{SEI,n}Fj_n \tag{15}$$

In Equation (15), $\eta_{ohm,p}$ represents the ohmic polarization potential of positive electrode, $\eta_{ohm,n}$ represents the ohmic polarization potential of negative electrode, $R_{SEI,p}$ represents the ohmic resistance

induced by SEI film of positive electrode, and $R_{SEI,n}$ is the ohmic resistance induced by SEI film of negative electrode. Combining the above-mentioned solid-phase diffusion process, reaction polarization process and ohmic polarization process, the terminal voltage of the battery can be expressed as follows.

$$U_t = E_p\left(\frac{c_{s,surf,p}}{c_{s,\max,p}}\right) - E_n\left(\frac{c_{s,surf,n}}{c_{s,\max,n}}\right) + \frac{2RT}{F}\frac{\ln\left(m_p + \sqrt{m_p^{\,2}+1}\right)}{\ln\left(m_n + \sqrt{m_n^{\,2}+1}\right)} + R_{SEI,p}Fj_p - R_{SEI,n}Fj_n \tag{16}$$

Based on the above equations, the SP model of lithium-ion battery with current as input and terminal voltage as output is established. The block diagram of the SP model is shown in Figure 2.

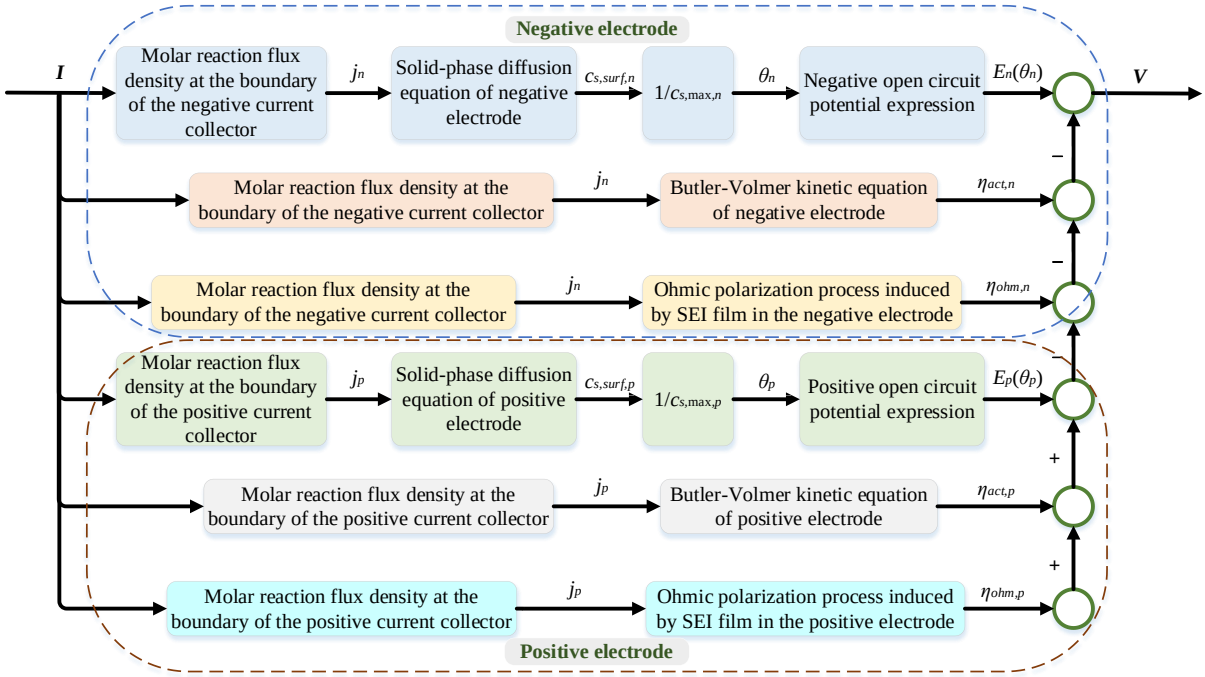

Figure 2. The block diagram of the SP model

As shown in Figure 2, the block diagram of the SP model consists of a positive module and a negative module. Among the parameters shown in Figure 2, I represents the input current, V represents the output voltage, θ_p is the ratio of the positive solid-phase surface lithium-ion concentration to the positive maximum solid-phase lithium-ion concentration, and θ_n is the ratio of the negative solid-phase surface lithium-ion concentration to the negative maximum solid-phase lithium-ion concentration.

2.2. LDW-PSO parameter identification

There are many parameters involved in the electrochemical model of lithium-ion battery, some of which cannot be measured by experiments. For the SP model, the maximum solid-phase lithium-ion concentrations of positive and negative electrodes are two of the most important electrochemical parameters, which directly affect the accuracy of the model and the states of the battery. In order to accurately obtain them under different degradation cycles, the LDW-PSO algorithm is selected to

identify the above parameters. The core idea of this parameter identification algorithm is to minimize the error between the measured voltage and the simulation voltage of the SP model. Therefore, the objective function of the LDW-PSO parameter identification algorithm is shown in the following formula.

$$\min J(\theta) = \sum_{i=1}^{n} \left[V_i - f(I_i, \theta) \right]^2, \theta = \left(c_{s,\max,p}, c_{s,\max,n} \right) \tag{17}$$

In Equation (17), V_i is the terminal voltage of the battery, I_i is the input current of the battery, $f(I_i, \theta)$ is the simulation terminal voltage output of the SP model, θ is the set of parameters to be identified in the SP model, i is the sampling point, and n is the maximum value of the sampling point. By combining the above objective function, the model parameter identification block diagram is shown in Figure 3.

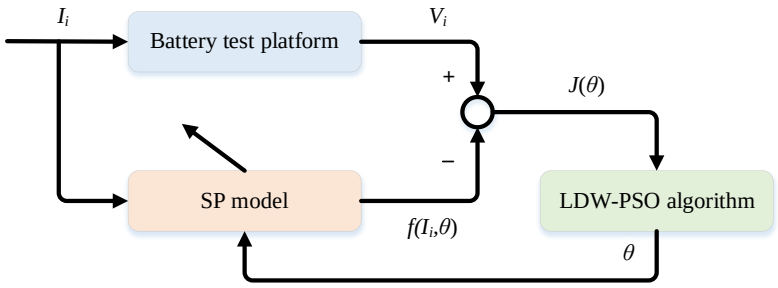

Figure 3. The model parameter identification block diagram

The particle swarm optimization (PSO) algorithm is a random search algorithm based on group cooperation. The basic idea of the algorithm is to find the optimal solution through cooperation and information sharing among individuals in the group. In a search space, a set of random particles is initialized first, and the positions of these random particles represent the current optimal solution. The quality of particle positions can be determined by the fitness value of the objective function. These particles continuously adjust the speed and direction of moving in the search space according to their previous search experience and group search experience, so that the particles can quickly search for the optimal solution.

The PSO algorithm can be used to solve optimization problems in continuous space. Each particle searches for the optimal solution with different speeds and directions in the search space, and it is recorded as the current individual optimal value of this particle. After one iteration of the algorithm, according to the fitness value, the optimal individual optimal value of all particles is found as the global optimal solution of the group, and it is recorded as the current global optimal value of the group. All particles in the group update their speed and position according to the current individual optimal value and global optimal value. The update expressions of particle speed and position in each search process is shown in the following formulas.

$$\begin{cases} v_i(k+1) = v_i(k) + c_1 r_1 \left(p_{best,i} - x_i(k) \right) + c_2 r_2 \left(g_{best} - x_i(k) \right) \\ x_i(k+1) = x_i(k) + v_i(k+1) \\ x_i = (x_{i1}, x_{i2}, \cdots x_{iD}), v_i = (v_{i1}, v_{i2}, \cdots v_{iD}) \\ p_{best,i} = (p_{best,i1}, p_{best,i2}, \cdots p_{best,iD}), g_{best} = (g_{best,1}, g_{best,2}, \cdots g_{best,D}) \end{cases} \quad (18)$$

Wherein, v_i represents the moving speed vector of the ith particle, x_i represents the position vector of the ith particle, p_{best} is the current individual optimal value of the ith particle, g_{best} is the current global optimal value of the group, k represents the current iteration number, r_1 and r_2 are random numbers from 0 to 1, c_1 and c_2 are learning factors, and D is the search space dimension. The first term on the right side of the speed update expression in Equation (18) is called the memory term, which represents the influence of the speed and direction at the previous moment on the speed at the current moment. The second term is called self-cognition term, which reflects the influence of self-experience on the current moving speed of particles. The third term is called the group cognition term, which reflects the cooperation and mutual influence among particles. Under the joint action of the above three parts, the global optimal solution can be found in the iterative process.

Although the PSO has the advantages of few adjustment parameters and fast calculation speed, the algorithm cannot meet the requirements in some cases. For example, if the proportion of the memory item is too large, particles will move at almost a fixed speed and direction during the search process until the search boundary. This can lead to missing the optimal solution during the search. If the proportion of the self-cognition item and the group cognition item is too large, the moving speed of particles in the search process is almost only determined by the individual optimal value and the group optimal value. In this case, if the fitness value corresponding to the initial moment of the particle is small, the moving speed of the particle is almost zero, which may lead to the local optimal solution as the result of the algorithm. Therefore, a dynamic weight factor w is introduced to improve the deficiency of PSO algorithm in this paper. The improved algorithm is called LDW-PSO algorithm. In the LDW-PSO algorithm, the position update expression is the same as the PSO algorithm, and the speed update expression is shown below.

$$v_i(k+1) = w v_i(k) + c_1 r_1 \left(p_{best,i} - x_i(k) \right) + c_2 r_2 \left(g_{best} - x_i(k) \right) \quad (19)$$

The weight factor w can characterize the ability of the particle to inherit the speed of the previous moment. A larger weight factor can make the particle run faster, which is beneficial to the global search, and a smaller weight factor can make the particle run slower, which is beneficial to the local search. In the initial stage of the search, enhancing the global search ability can increase the probability of traversing the solution space to prevent the algorithm from falling into the local optimal solution. In the later stage of search, enhancing the local search ability can increase the probability of finding the global optimal solution. Therefore, setting the appropriate weight factor can make the algorithm search the optimal solution accurately and quickly. In order to better balance the global search and local search ability of the algorithm, a linear decreasing function about the number of iterations is used to represent the dynamic change of the weight factor. The expression of the weight factor is shown in the following formula.

$$w = w_{\max} - \frac{w_{\max} - w_{\min}}{k_{iter}} k \quad (20)$$

Wherein, w_{max} is the maximum value of weighting factor, w_{min} is the minimum value of weighting factor, k is the current number of iterations, and k_{iter} represents the maximum number of iterations. The flowchart of the LDW-PSO algorithm is shown in Figure 4.

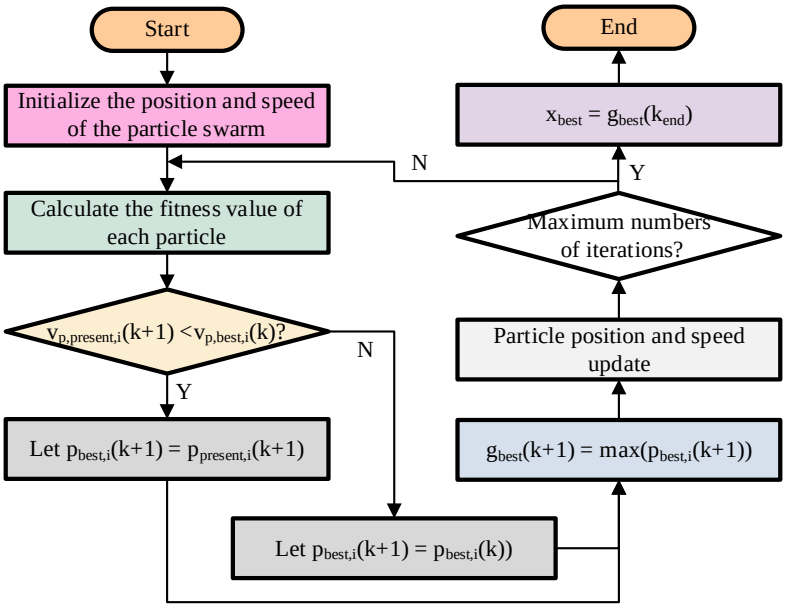

Figure 4. The flowchart of the LDW-PSO algorithm

In Figure 4, $v_{p,present,i}(k+1)$ represents the fitness value calculated by the ith particle at $k+1$ iterations, $v_{p,best,i}(k)$ represents the fitness value corresponding to the optimal solution of the ith particle at k iterations, $p_{present,\ i}(k+1)$ represents the position of the ith particle at $k+1$ iterations, $p_{best,i}(k+1)$ represents the optimal solution of the ith particle at $k+1$ iterations, $g_{best}(k+1)$ represents the global optimal solution at $k+1$ iterations, k_{end} represents the number of the last iteration, and x_{best} represents the global optimal solution of the final output.

The main process of identifying the maximum solid-phase lithium-ion concentration in the positive and negative electrodes by LDW-PSO algorithm can be summarized as the following six steps:

(1) Set the number of particle swarm, randomly assign the initial position and speed of each particle in the search area, and take the particle position as the initial individual optimal solution p_{best};

(2) The fitness value of each particle in this iteration is calculated according to the objective function;

(3) For each particle, the fitness value of this iteration is compared with the minimum fitness value of the last iteration, and the position with lower fitness value is assigned to the individual optimal solution p_{best};

(4) The maximum of all individual optimal values in this iteration is taken as the global optimal value in this iteration;

(5) The speed and position of each particle is updated. It should be noted that if the updated particle position or speed is beyond the set range, the corresponding boundary value will be assigned to the particle;

(6) If the maximum number of iterations is not reached, steps (2) to (5) need to be looped. The global optimal value when the iteration stops is the final result of parameter identification.

2.3. Quantification method of degradation modes based on IC-DV

In different environments, the open circuit voltage curves during constant current charging are basically flat and overlapping, and it is difficult to directly distinguish the differences between the curves. The IC-DV method can convert the flat stages in the open circuit voltage curve into the dQ/dU value of the IC curve and the dU/dQ value of the DV curve. By analyzing the changes of the IC curve and the DV curve, the relationship between the external characteristics and the internal electrochemical characteristics of the battery can be established.

The IC method is a method to analyze the degradation characteristics of batteries based on the IC curve. In practical applications, the differential dQ/dU of capacity to voltage is replaced by the ratio of incremental capacity Q to voltage step U. Therefore, the expression of IC method is shown in the following formula.

$$IC = \frac{\Delta Q}{\Delta U} \tag{21}$$

It can be seen from the Equation (21) that the acquisition of the IC curve needs the support of the capacity-voltage curve, so it is necessary to charge or discharge the battery at a low rate. The reason for not using high-rate current is that under high-rate conditions, lithium ions cannot be fully intercalated and deintercalated, resulting in changes in battery performance. At the same time, a high rate will lead to an increase of the polarization current of the battery, resulting in an increase of the internal resistance of the battery and the early arrival of the cut-off voltage for charge and discharge, which is manifested as a decrease of the capacity of the battery.

The peaks in the IC curve can represent the most obvious incremental capacity changes, and they can characterize the structural features and material changes inside the lithium-ion battery to a certain extent. In addition, the peak points of the IC curve are in the flat stages of the battery discharge curve, which can characterize the sensitivity of the battery to capacity changes during the smooth discharge process.

On the other hand, The DV method is another method to analyze the degradation characteristics of batteries based on the DV curve. In practical applications, the differential dU/dQ of voltage to capacity is replaced by the ratio of voltage step U to incremental capacity Q. Therefore, the expression of DV method is shown below.

$$DV = \frac{\Delta U}{\Delta Q} \tag{22}$$

It can be seen from the Equation (22) that, similar to the IC curve, the acquisition of the DV curve also needs the support of the capacity-voltage curve, so it is also necessary to charge or discharge the battery at a low rate. The values and positions of peaks in the DV curve can characterize the internal changes of lithium-ion batteries to some extent, and they can reflect the sensitivity of lithium-ion batteries to voltage changes. From the above description, it can be seen that DV and IC are two opposite concepts.

Since the IC-DV method is introduced to quantify the degradation modes, the changes of IC-DV curves under different ratios and temperatures are not considered, but only the changes of IC-DV curves under different degradation degrees are considered. degradation mode is an upper concept of degradation mechanism. The definition of the degradation mode is a collection of degradation mechanisms with the same cause or form. A degradation mode generally includes many degradation mechanisms. The degradation modes of lithium-ion batteries mainly contain loss of lithium inventory (LLI), loss of active material (LAM), and conductivity loss (CL).

The active lithium ions are the lithium ions that complete the process of intercalation and deintercalation from the electrodes in the normal operation, and the reduction of active lithium ions is characterized by the capacity degradation of the battery. The LLI degradation modes contain the formation and changes of solid electrolyte interphases (SEI), electrolyte degradation side reactions, and lithium deposition, etc. The active material acts as a carrier for lithium ions intercalated into the electrodes during the reaction process. Therefore, the LAM can also indirectly lead to the degradation of battery capacity. The LAM degradation modes contain physical damage of active materials, chemical reaction decomposition of active materials, and contact isolation of active materials, etc. The CL mainly characterizes the power degradation of lithium-ion batteries, so it is not mentioned in this paper. During the cycles of battery, battery degradation will be caused by LAM, LLI and other reasons. Under the same working condition, the electrochemical reaction of the battery at different degradation degrees is different. The intercalation and deintercalation of lithium ions at the positive and negative electrodes can lead to changes in battery performance, which will affect the open circuit voltage curve and capacity of the battery.

By analyzing the characteristics of IC-DV curves of batteries with different degradation degrees, the degradation modes and mechanisms of battery can be obtained, which is helpful for diagnosing the SOH of batteries. Carlos et al.[38] and David et al.[39] pointed out that the LAM degradation modes are mainly reflected in the change of the left peaks of the IC curve. Meinert et al.[40] believed that the LLI degradation modes can be reflected to some extent by the offset of the DV curve along the coordinate axis.

Therefore, a quantification method of degradation modes based on IC-DV is proposed in this paper. The quantification expression of LAM and LLI is shown in the following formulas.

$$\begin{cases} LAM = \dfrac{\dfrac{\Delta Q_{IC}}{\Delta U_{IC}} - \dfrac{\Delta Q_{IC}}{\Delta U_{IC}}|1}{\dfrac{\Delta Q_{IC}}{\Delta U_{IC}}|1} \\ LLI = \dfrac{Q_{DV} - Q_{DV,1}}{Q_{DV,1}} \end{cases} \tag{23}$$

In Equation (23), $\frac{\Delta Q_{IC}}{\Delta U_{IC}}$ is the peak value of the most obvious peak on the left side of the IC curve, $\frac{\Delta Q_{IC}}{\Delta U_{IC}}|1$ is the peak initial value of the most obvious peak on the left side of the IC curve, Q_{DV} is the rightmost capacity value in the DV curve, and $Q_{DV,1}$ is the initial value of the rightmost capacity value in the DV curve. The quantification method of degradation modes based on IC-DV can analyze the degradation characteristics and the changing trend of battery degradation modes from the perspective of

time domain. Figure 5 is the schematic diagram of the quantification process.

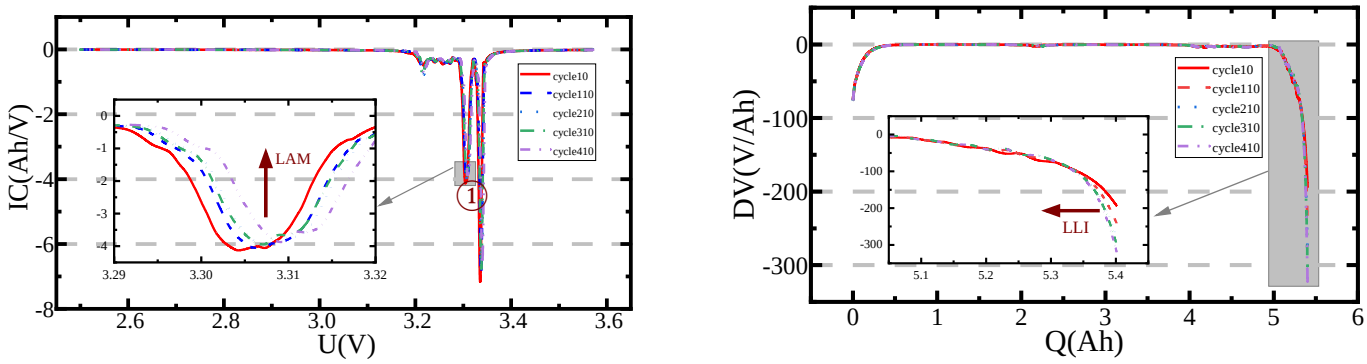

(a) Schematic diagram of quantification of LAM in IC curves

(b) Schematic diagram of quantification of LLI in DV curves

Figure 5. The schematic diagram of the quantification process

It can be seen from Figure 5 that Figure 5(a) is a quantification diagram of the LAM in the IC curves, peak① marked in Figure 5(a) is the most obvious peak on the left, and Figure 5(b) is a quantification diagram of the LLI in the DV curves.

2.4. Grey relational analysis

In order to improve the training efficiency of BPNN model and the accuracy of SOH estimation results, it is necessary to select parameters closely related to battery degradation as the input of BPNN. The grey relational analysis (GRA) method is used to analyze whether the maximum solid-phase lithium-ion concentration of positive and negative electrodes, LLI and LAM are suitable as input parameters of BPNN. In this paper, it can be known from the capacity definition method of SOH that the capacity sequence can be used as a reference sequence. The capacity definition expression of SOH is shown in the following formula.

$$SOH = \frac{Q}{Q_{rate}} \tag{24}$$

In Equation (24), Q represents the current capacity of the battery, and Q_{rate} represents the rated capacity of the battery. Under the same independent variable, the magnitude of the relation between the changes of the two sequences is called the relational degree. The more similar the variation trends of the sequences, the greater the relation between the corresponding sequences. The GRA method is a method to quantify the development trend of the system. Its basic idea is to reflect the relational degree between sequences by comparing the curve shape similarity between the reference sequence and comparison sequences. Among them, the reference sequence is used to characterize the behavior of the system, and the comparison sequences are the related sequences that affect the behavior of the system. Furthermore, the GRA method is also suitable for small and irregular samples. This method has a small amount of calculation, and there is no discrepancy between the quantitative results and the qualitative analysis

results. Therefore, the GRA method is adopted to analyze the relevant parameters of the battery degradation process. The GRA method includes the following four steps:

(1) The first step is searching and determining reference and comparison sequences. In this paper, the reference sequence is the change sequence of lithium battery capacity with degradation cycles, and the comparison sequence are the sequences of the maximum solid-phase lithium-ion concentration of positive and negative electrodes, LAM and LLI with degradation cycles. The expressions of the reference sequence and the comparison sequence are shown in the following formulas.

$$\begin{cases} X_i = \left\{ x_i(k) \mid k = 1, 2, ..., n \right\} \\ Y = \left\{ y(k) \mid k = 1, 2, ..., n \right\} \end{cases} \tag{25}$$

In Equation (25), X and Y represent the comparison sequence and the reference sequence, respectively. Besides, i is the sequence number of the comparison sequence, k is the sequence number of each point in the sequence, and n represents the length of the sequence.

(2) The second step is performing dimensionless processing of reference and comparison sequences. Since the physical meaning of each sequence in the system may be different, the data dimension may also be different, which will lead to inconvenient comparison between sequences. Therefore, it is generally necessary to carry out dimensionless processing of the data in the GRA. The dimensionless processing methods mainly include initial value processing, mean value processing and normalization processing. In this paper, the maximum-minimum normalization method is selected. This method can transform the sequence linearly so that the data can be transformed to between 0 and 1. The specific expression of it is shown below.

$$x_{trans} = \frac{x - \min}{\max - \min} \tag{26}$$

Wherein, x is a value in the sequence, x_{trans} is the dimensionless value of x, max is the maximum value in the sequence, and min is the minimum value in the sequence.

(3) The third step is calculating the relational coefficient between the reference sequence and the comparison sequence. The relational degree is essentially the degree of difference in the shape of the curves. Therefore, the difference between the curves can be used as a quantitative indicator of the relational degree. The calculation expression of the relational coefficient is shown in the following formulas.

$$\begin{cases} \xi_i(k) = \dfrac{\min\limits_i \min\limits_k \Delta_i(k) + \rho \min\limits_i \min\limits_k \Delta_i(k)}{\Delta_i(k) + \rho \min\limits_i \min\limits_k \Delta_i(k)} \\ \Delta_i(k) = \left| y(k) - x_i(k) \right| \end{cases} \tag{27}$$

In Equation (27), ξ is the relational coefficient between each comparison sequence and the reference sequence at each point, ρ is the resolution coefficient, and its value is usually 0.5.

(4) The last step is calculating the relational degree between the reference sequence and the comparison sequence. It can be seen from step (3) that the relational coefficient only compares the magnitude of the relation between the sequence and the reference sequence at each point, so the relational coefficient cannot be used for overall comparison. Thence, the concept of relational degree is proposed, and the relational degree is the mean value of the relational coefficient under the corresponding comparison sequence. The calculation expression of the relational degree is shown below.

$$r_i = \frac{1}{n}\sum_{i=1}^{n}\xi_i(k), (k = 1, 2, ..., n) \quad (28)$$

In Equation (28), *i*, *k* and *n* represent the same meanings as in Equation (25), and *r* is the relational degree. The closer the value of *r* is to 1, the more related the reference sequence is to the comparison sequence.

2.5. BP neural network

Neural network is a model that simulates the structure and characteristics of the brain for data processing. It originates from the nervous system of animals and has the advantages of high fault tolerance, strong adaptability, strong anti-interference ability and strong self-learning ability. Neural networks do not need to understand the system. They can automatically obtain the system characteristics in the process of data training and simulate the nonlinear mapping relationship between the input and output of the system by learning.

The parallel structure of neural network enables each neuron to perform independent operations and processing according to the received information, which greatly improves the running speed. BPNN is a simple and practical neural network model, which is often used to solve the problems of nonlinear systems. Due to the nature of the internal electrochemical reaction, the battery is a highly complex nonlinear system. In this paper, the BPNN with the maximum solid-phase lithium-ion concentration of the positive and negative electrodes, LLI and LAM as the input is used to map the battery for realizing the estimation of the battery SOH.

The characteristics of BPNN are mainly determined by its structure and learning rules. The BP neural network is structurally represented as forward feedback learning, and feedback learning runs through the whole structure. The BP algorithm includes two processes of signal forward propagation and error back propagation. During forward propagation, the input signal acts on the output node through the hidden layer, and the output signal is generated through nonlinear transformation. If the actual output does not match the expected output, it will turn into the back propagation process of the error. The back propagation of the error is that the output error is transmitted layer by layer to the input layer through the output layer, and the error is allocated to all nodes in each layer. By using the error signals obtained by each layer as the basis for adjusting the weights of each connection, the weights from the hidden layer to the output layer and from the input layer to the hidden layer are adjusted in turn to achieve the optimal value of the error objective function. The schematic diagram of the three-layer BPNN model is shown in Figure 6.

It can be seen from Figure 6 that the BPNN model includes the input layer, the hidden layer and the output layer. The neural networks between the adjacent layers are completely connected to each other, and the neurons in the same layer are independent of each other.

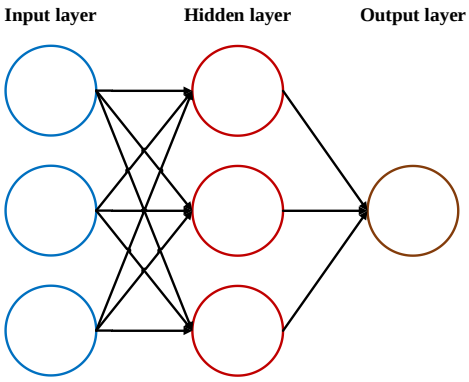

Figure 6. The schematic diagram of the three-layer BPNN model

The neuron is the basic structure in the neural network model, which contains the information of the connection chain, the adder and the transfer function. There is no direct connection between neurons and the outside world, but the change of their states can affect the relationship between input and output. The input and output relationship between the adjacent layers of the BPNN is shown in the following formulas.

$$\begin{cases} net_j = \sum_{i=1}^{n} w_{ij} x_i - \theta \\ y_j = f\left(net_j\right) \end{cases} \tag{29}$$

In Equation (29), x_i is a signal from other neurons or information from outside. And w_{ij} represents the connection weight from neuron i to neuron j, which indicates the connection strength between neurons. The value of w_{ij} usually changes dynamically, which is determined by the learning process of the neural network. The product of x_i and w_{ij} is the input value from neuron i to neuron j, which represents the connection chain mentioned above. Besides, θ is the internal threshold of neurons, and $f(\bullet)$ represents the transfer function. The most common transfer functions include linear functions and nonlinear functions such as Sigmoid functions. Generally speaking, the transfer function of the hidden layer is a nonlinear function, and the transfer function of the output layer is a linear function. In addition, net_j represents the weighted input to the neuron j, y_j represents the output value of neuron j mapped by BPNN, and n is the number of neurons input to neuron j.

Learning rules are methods for adjusting the weights of network links between neurons, and only supervised learning methods can formulate learning rules. Learning methods are divided into fixed memory learning methods, unsupervised learning methods and supervised learning methods. The connection weights in the fixed memory learning method are constant, so the corresponding model accuracy is low. Connection weights in unsupervised learning methods adjust autonomously but are not affected by feedback signals. In each supervised learning method, an evaluation criterion is set as a learning rule, and the connection weights are adjusted through feedback signals to improve the model accuracy. Common learning rules include gradient descent method, quasi-Newton method and Levenberg-Marquardt (LM) method. The optimal principle, also called loss function, is usually chosen as the conventional square error function.

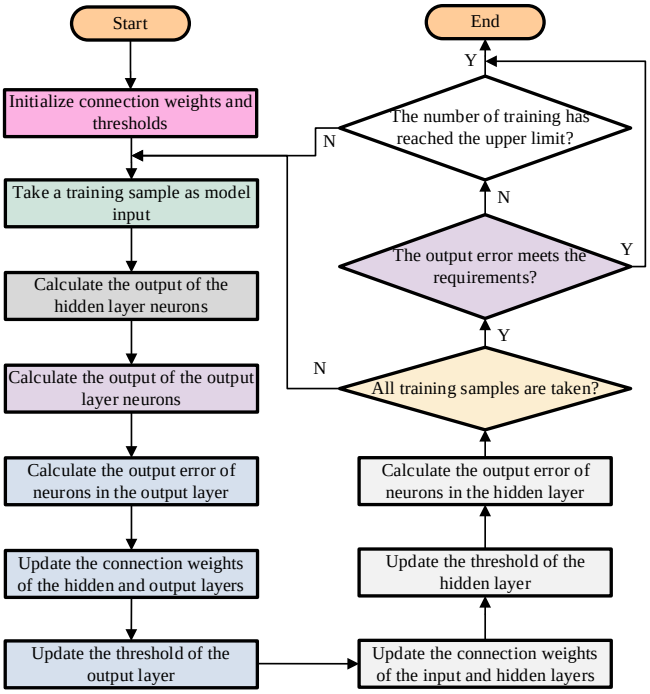

Figure 7. The flowchart of the BPNN training process

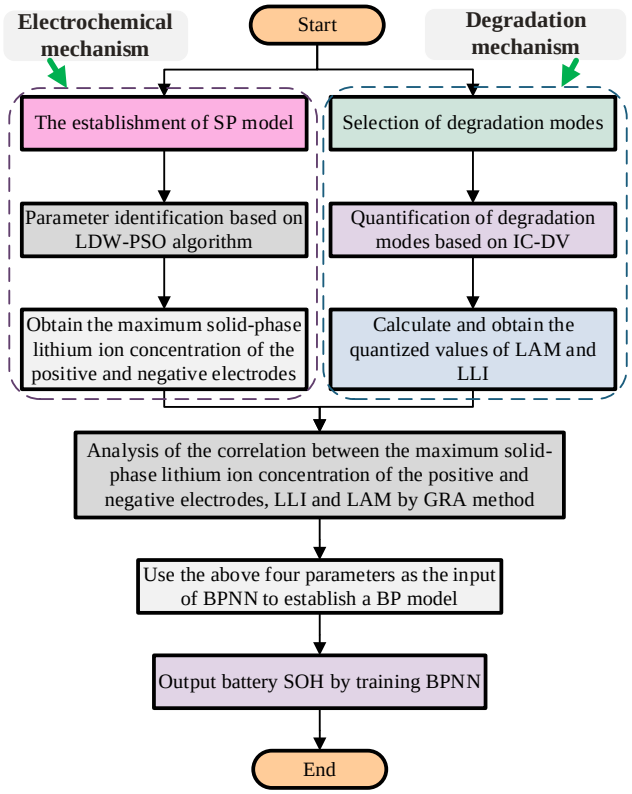

Figure 8. The flowchart of the lithium-ion battery SOH estimation method

The loss function of BPNN is shown below.

$$E = \frac{1}{2}\sum_{k=1}^{N}\left(y_{t,k} - y_{BP,k}\right)^2 \tag{30}$$

In Equation (30), $y_{t,k}$ is the actual value of the model output, $y_{BP,k}$ is the estimated value of the model output, and N is the number of neurons in the output layer. When i and j in Equation (28) represent neurons in the hidden layer and output layer, respectively, $y_{t,k}$ is y_j. The flowchart of the BPNN training process is shown in Figure 7.

As can be seen from Figure 7, after all training samples are taken out, the output error of BPNN and the maximum number of training times determine whether the network stops. Moreover, Figure 7 also shows that the feedback information can help BPNN to continuously update the connection weights and thresholds. Combined with the SP modeling, LDW-PSO parameter identification, quantification method of degradation modes based on IC-DV, GRA and BPNN, the flowchart of the lithium-ion battery SOH estimation method proposed in this paper is shown in Figure 8.

It can be seen from Figure 8 that the SOH algorithm proposed in this paper takes into account both the electrochemical mechanism and the degradation mechanism. And on this basis, parameters with a high relational degree with capacity are extracted as the input of BPNN for model training to obtain the SOH in the battery degradation process.

In addition to the estimation method proposed in this paper, some scholars have adopted similar models regarding SOH estimation of energy storage in lithium-ion batteries. Park proposed a method for estimating and predicting SOH when the amount of measured data is insufficient by combining a dual extended Kalman filter and a multivariate autoregressive model[34]. The focus of this method is to predict the SOH, and only the dual extended Kalman filter is used to estimate the SOH, resulting in a low accuracy of the estimation result. Zhang studied a method for SOH estimation based on coulomb counting method and differential voltage analysis[41]. In document [41], only the fast estimation of SOH in the constant current discharge stage is verified, and the method is not based on any physical model, which has lower interpretability than the method proposed in this paper. Kaveh developed a method for SOH estimation based on enhanced single particle model (ESPM) parameter estimation[42]. It can be seen from document [42] that all the experimental process and verification process are carried out under the electric vehicle data, so there is no basis to judge the pros and cons of this method to estimate the battery SOH in the energy storage system. And compared with the algorithm proposed in this paper, the SOH mentioned in [42] is obtained by fitting with characteristic parameters, so the anti-interference performance of this method is poor.

Tan[43] and Xiong[23] proposed SOH estimation methods based on SVM and weighted least squares-support vector machine (WLS-SVM), respectively. The former adopted the extended Kalman filter-recursive least squares (EKF-RLS) method to identify the parameters in the second-order RC equivalent circuit model, and used the RC values at different states of charge as the input of the SVM to estimate the SOH. Since all ECMs can only describe the external characteristics of batteries, the accuracy of the method proposed by Tan is lower than that of the method proposed in this paper. The latter estimated the SOH by extracting the characteristic parameters closely related to the SOH in the battery charging curve as the input of the WLS-SVM model. The method is not based on the battery physical model and internal mechanism, so it has lower interpretability than the method proposed in this paper.

3. EXPERIMENTAL ANALYSIS

3.1. Test platform and experimental setup

All the experimental procedures mentioned in this paper were carried out in a power battery high-rate charge-discharge tester (BTS750-200-100-4) and a temperature-controlled chamber thermostat (DGBELL-BTKS). In addition, the charge-discharge tester is connected to a high-configured computer for storing and calculating battery experimental data. The experimental platform is shown in Figure 9.

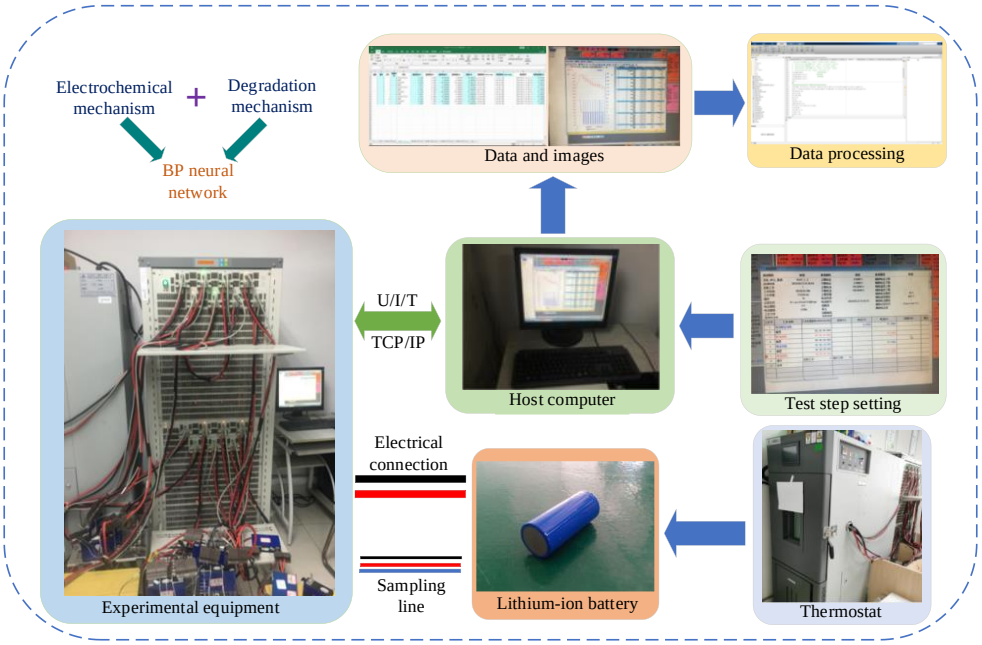

Figure 9. Test platform

In this paper, experimental studies were performed on a commercial 26650 graphite/LFP cell with a rated capacity of 2.3 Ah and the experimental temperature of the thermostat was set to 25 °C. Based on the hardware foundation of the above-mentioned experimental platform, corresponding experiments can be carried out on the cell.

In this paper, the experiments to be completed include cyclic degradation experiments, capacity test experiments and low current discharge experiments. In order to simulate the degradation of the test battery in the working environment of the energy storage power station, a cyclic degradation experiment is customized according to the actual discharge conditions of the battery in the energy storage power station. In each cycle test, the energy storage battery goes through the process of discharge, shelving and charging. Among them, the discharge condition is basically constant in a certain period of time, and the charging condition contains constant current and constant voltage. During this experiment, the charge-discharge current is the same between each cycle. The current curve within one degradation cycle is shown in Figure 10.

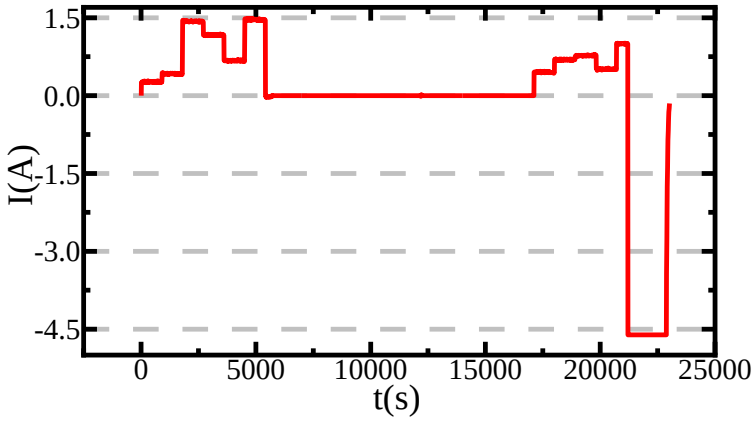

Figure 10. The current curve within one degradation cycle

In Figure 10, the positive current represents the discharge process and the negative current represents the charging process. The current of constant current charging is 2C, and C represents the rated capacity of the cell. In order to measure battery characterization data on a regular basis, a characteristic test is performed every ten degradation cycles. The characteristic test includes the above-mentioned capacity test experiment and low current discharge experiment. The capacity test experiment consists of the following five steps:

(1) The cell is charged to full with 1/3C constant current and constant voltage. The cutoff voltage is 3.6V and the cutoff current is 20/C.

(2) Let the cell rest for 30 minutes after charging.

(3) The cell is discharged with 1C constant current. The cutoff voltage is 2.5V.

(4) Let the cell rest 30 minutes after discharging.

(5) Repeat the above steps three times.

The mean capacity value obtained from the three capacity test experiments represents the maximum capacity value of the cell under this degradation cycle. In this paper, since the battery has been fully charged through the constant current and constant voltage charging process after each cycle, step (1) was skipped during the first capacity test experiment. In addition, the low current discharge experiment was carried out after the end of the capacity test experiment. There are two steps in the low current discharge experiment. First, the cell is charged to the upper limit cut-off voltage with a current of 1/3C. Then, the cell is discharged to the lower cut-off voltage with a current of C/20 after shelving for 1 hour.

3.2. Identification results and model verification

In this paper, it is necessary to identify the maximum solid-phase lithium-ion concentration of positive and negative electrodes in each degradation cycle. Therefore, the discharge process in each cycle is selected to establish the SP model, and the discharge current curve can be seen from Figure 10. At the same time, it can be known from Equation (2) that in order to calculate the battery terminal voltage, it is

necessary to obtain the positive and negative open circuit potential expressions. Empirical expressions for the same type of batteries are used here. The expressions of the negative open circuit potential and the positive open circuit potential are shown below.

$$\begin{cases} E_n\left(\theta_{s,n}\right)=0.6379+0.5416e^{-305.5309\theta_{s,n}}+0.044\tanh\left(\frac{-\left(\theta_{s,n}-0.1958\right)}{0.1088}\right)-0.1978\tanh\left(\frac{\theta_{s,n}-1.0571}{0.0854}\right) \\ -0.6875\tanh\left(\frac{\theta_{s,n}+0.0117}{0.0529}\right)-0.0175\tanh\left(\frac{\theta_{s,n}-0.5692}{0.0875}\right),\theta_{s,n}=\frac{c_{s,surf,n}}{c_{s,\max,n}} \\ E_p\left(\theta_{s,p}\right)=3.4323-0.8428e^{\left(-80.2493\left(1-\theta_{s,p}\right)^{1.3198}\right)}-3.2494*10^{-6}e^{\left(20.2645\left(1-\theta_{s,p}\right)^{3.8003}\right)} \\ +3.2482*10^{-6}e^{\left(20.2646\left(1-\theta_{s,p}\right)3.7995\right)},\theta_{s,p}=\frac{c_{s,surf,p}}{c_{s,\max,p}} \end{cases} \quad (31)$$

According to Equation (31), the open circuit potential curves of the positive and negative electrodes can be obtained, which is shown in Figure 11.

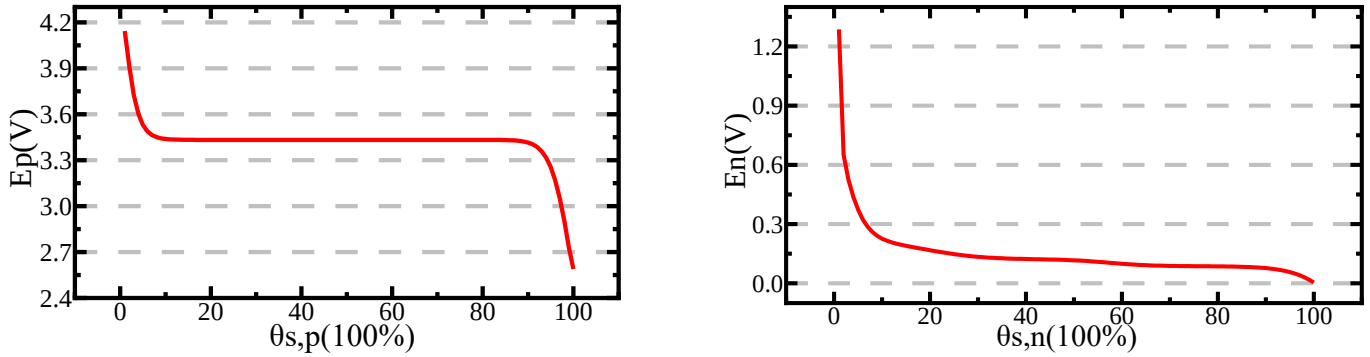

(a) The open circuit potential curve of the positive electrode

(b) The open circuit potential curve of the negative electrode

Figure 11. The open circuit potential curves of the positive and negative electrodes

As can be seen from Figure 11, Figure 11(a) shows the positive open circuit potential curve, and Figure 11(b) shows the negative open circuit potential curve. And it is known from Equation (16) that in addition to the expression of positive and negative open circuit potential, the establishment of SP model also needs to obtain some internal parameters of the cell. In this paper, the specific values of the relevant parameters in the SP model are shown in Table 1.

Table 1. The relevant parameters in the SP model

Parameter	LFP (positive electrode)		Graphite (negative electrode)	
	Symbol	Value (25℃)	Symbol	Value (25℃)
The radius of the active particle (m)	$R_{s,p}$	3.65×10^{-8}	$R_{s,n}$	3.5×10^{-6}
Solid-phase diffusion coefficient (m^2/s)	$D_{s,p}$	1.18×10^{-18}	$D_{s,n}$	2×10^{-14}
Material porosity	ε_p	0.3	ε_n	0.47
Filling substance volume fraction	$\varepsilon_{f,p}$	0.26	ε_n	0.03
Plate thickness (m)	l_p	70×10^{-6}	l_n	34×10^{-6}

Effective area of pole piece (m^2)	A_p	0.17	A_n	0.17
Ohmic resistance induced by SEI film ($\Omega \cdot m^2$)	$R_{SEI,p}$	0.001	$R_{SEI,n}$	0.001
Average electrode reaction rate constant ($m^{2.5}mol^{-0.5}s^{-1}$)	k_p	3×10^{-11}	k_n	8.19×10^{-12}
Liquid-phase lithium-ion concentration (mol/m^3)	$c_{e,p}$	1000	$c_{e,n}$	1000
Initial surface lithium-ion concentration of solid-phase particle (mol/m^3)	$c_{s,surf,0,p}$	3900	$c_{s,surf,0,n}$	14870
Faraday constant (C/mol)	F	96487	F	96487
Universal gas constant (J/mol/K)	R	8.314	R	8.314
Battery temperature (K)	T	298.15	T	298.15

By substituting the parameters shown in Table 1 into the SP model, an expression of the terminal voltage about the maximum solid-phase lithium-ion concentration of the positive and negative electrodes can be obtained. The LDW-PSO algorithm is used to identify the maximum solid-phase lithium-ion concentration of positive and negative electrodes. In this paper, the parameter settings in the LDW-PSO algorithm are shown in Table 2.

Table 2. The parameter settings in the LDW-PSO algorithm

Parameter	Symbol	Value	Unit
The maximum solid-phase Li-ion concentration of the positive electrode	$c_{s,max,p}$	[16000,27000]	(mol/m^3)
The maximum solid-phase Li-ion concentration of the negative electrode	$c_{s,max,n}$	[25000,36000]	(mol/m^3)
The maximum number of iterations	k_{iter}	500	/
The maximum value of weighting factor	w_{max}	0.9	/
The minimum value of weighting factor	w_{min}	0.4	/
Learning factor	c_1	2	/
Learning factor	c_2	2	/
Particle swarm size	m	20	/

By combining the SP model parameters shown in Table 1 and the LDW-PSO parameters shown in Table 2, the maximum solid-phase lithium-ion concentration ($c_{s,max,i}$) of positive and negative electrodes can be identified. The identification results of $c_{s,max,i}$ during the degradation cycles are shown in Figure 12.

It can be seen from Figure 12 that with the increase of the number of degradation cycles, the maximum solid-phase lithium-ion concentration of the positive and negative electrodes shows a decreasing trend. In order to verify the identification results and the SP model, the discharge condition of the first degradation cycle is used in this experiment to simulate the terminal voltage of the cell, and it is compared and analyzed with the reference value of the actual terminal voltage. The terminal voltage curves and the error between them are shown in Figure 13.

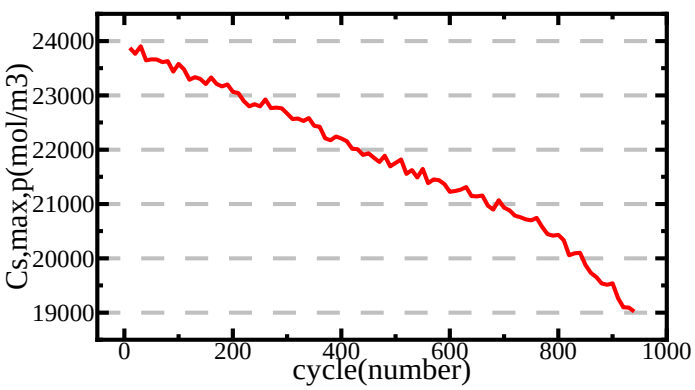

(a) The identification results of $c_{s,max,p}$

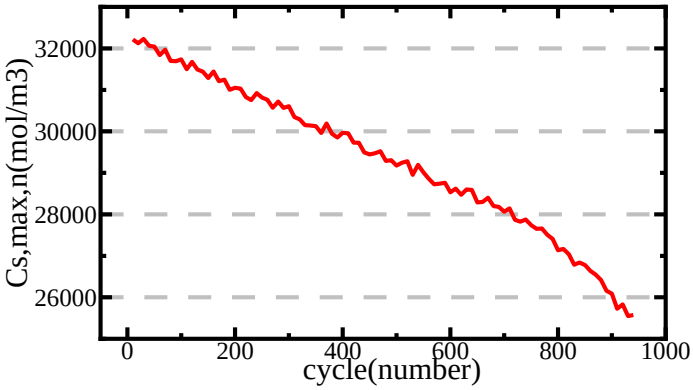

(b) The identification results of $c_{s,max,n}$

Figure 12. The identification results of $c_{s,max,i}$

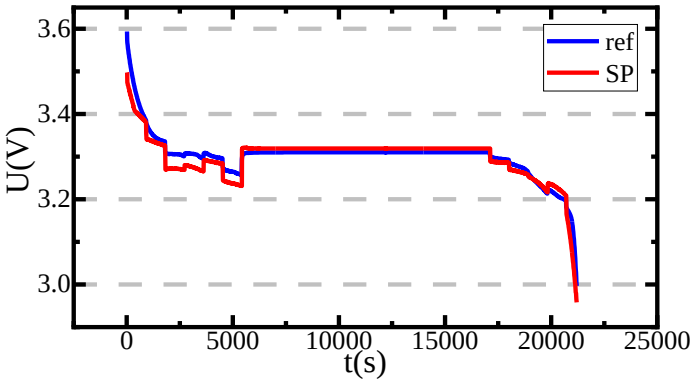

(a) The actual terminal voltage and SP model terminal voltage

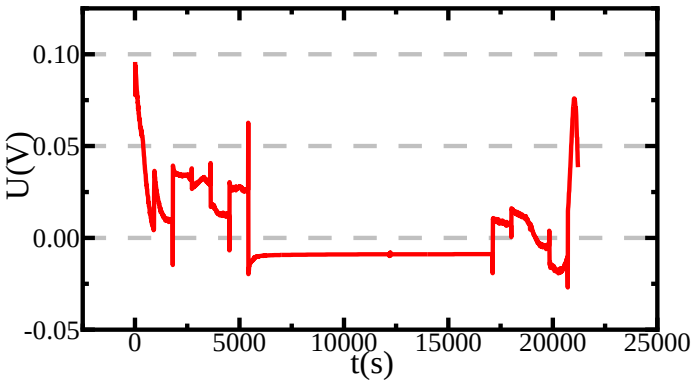

(b) The error of terminal voltages

Figure 13. The terminal voltage curves and the error between them

Figure 13(a) shows the actual terminal voltage and SP model terminal voltage and Figure 13(b) shows the error of the above voltages. It can be seen from them that the maximum error of the terminal voltage simulated by the SP model is less than 0.1 V, and the mean error outside the shelving time is 0.022 V. Besides, the mean square error (MSE) of the above voltages is 0.039%. The results show that the SP model can effectively simulate the cell under this condition.

3.3. Quantitative results of degradation modes

The quantitative formulas of the LAM and LLI degradation modes are shown in Equation (23). It is necessary to use IC and DV curves in the process of quantifying LAM and LLI. Among them, the constant ΔV taken in the IC curve is 0.001V, and the constant ΔQ taken in the DV curve is 0.002Ah.

During the degradation cycles of the cell, the quantitative results of LAM and LLI are shown in Figure 14.

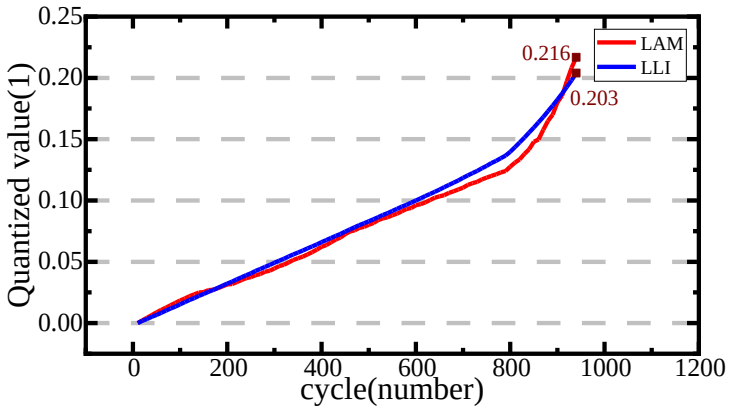

Figure 14. The quantitative results of LAM and LLI

The quantitative results of LAM and LLI are shown in Figure 14. Both LAM and LLI are the main causes of battery degradation. It can be seen from Figure 14 that there is little difference between the quantitative results of LAM and LLI during the process of battery degradation, and both have an increasing trend in the later stage of degradation. This feature reflects the nonlinear capacity degradation characteristic of the experimental cell after 800 degradation cycles.

3.4. Relational degree analysis

In order to analyze the relational degree of positive and negative maximum solid-phase lithium-ion concentration, LAM, LLI and the battery capacity, the positive and negative maximum solid-phase lithium-ion concentration, the negative value of LAM and the negative value of LLI are taken as the comparison series. In addition, the battery capacity is taken as the reference sequence, then the GRA method is used to calculate the corresponding relational degree. In the following data analysis, the negative values of LAM and LLI were considered as LAM and LLI, respectively. During the degradation cycles, the capacity degradation curve of the test cell can be obtained from the capacity test experiment, as shown in Figure 15.

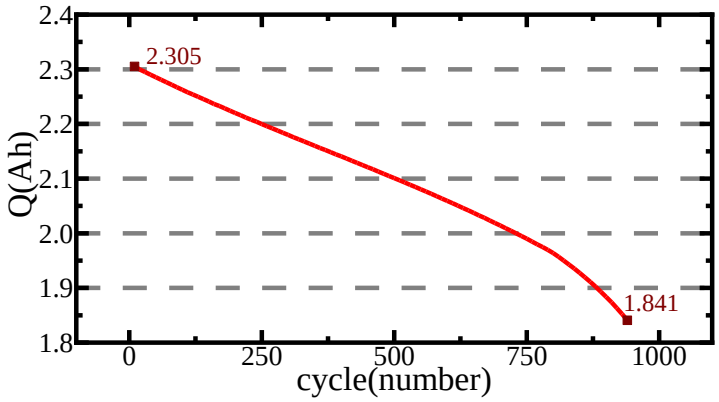

Figure 15. The capacity degradation curve of the test cell

Combined with the capacity degradation curve shown in Figure 15 and the maximum solid-phase lithium-ion concentration curve of the positive and negative electrodes shown in Figure 13, it can be seen that there is an obvious relation between them. It can be known from Figure 14 and Figure 15 that there is also a strong relation between the negative values of LAM and LLI and the capacity degradation curve. In order to analyze the relation between the above-mentioned comparison sequences and the reference sequence, it is necessary to calculate and sort the relational degree of each comparison sequence to evaluate the relation between $c_{s,max,p}$, $c_{s,max,n}$, LAM, LLI and battery capacity. The relational degree between the above parameters and the battery capacity is shown in Table 3.

Table 3. The relational degree between $c_{s,max,p}$, $c_{s,max,n}$, LAM, LLI and battery capacity

Parameter	Relational degree
$c_{s,max,p}$	0.8449
$c_{s,max,n}$	0.8661
LLI	0.7611
LAM	0.7182

It can be seen from Table 3 that the relation between $c_{s,max,p}$, $c_{s,max,n}$, and battery capacity is greater than that between LLI, LAM and battery capacity. The reason may be that LAM and LLI are only quantified by the characteristic curve and cannot accurately characterize the actual loss value of active materials and lithium inventory. In addition, it can be known from Table 3 that the relational degree between LAM and capacity is the smallest. This result may be caused by the fact that the loss of the active material does not dominate the whole degradation modes during the nonlinear degradation stage of the battery capacity. In general, the above four parameters are highly correlated with capacity and are suitable for estimating SOH as the input of neural network.

3.5. SOH analysis under the complex condition

It can be known from the above that the experimental cell has undergone a total of 940 aging cycles, so 94 sets of data with $c_{s,max,p}$, $c_{s,max,n}$, LAM and LLI as input and battery SOH as output are correspondingly obtained. Among the 94 sets of data, 84 sets of data were randomly selected as the training data of BPNN, and the other 10 sets of data were used as test data. In this paper, the input layer of BPNN includes four nodes, the hidden layer includes five nodes, and the output layer includes one node. The LM method is selected as the learning rule, the learning rate is set to 0.01, the maximum number of iterations is set to 100, and the target MSE is set to 1×10^{-5}. When the number of iterations exceeds the set value or the target MSE meets the requirement, the training is stopped. The training process of BPNN is shown in Figure 16.

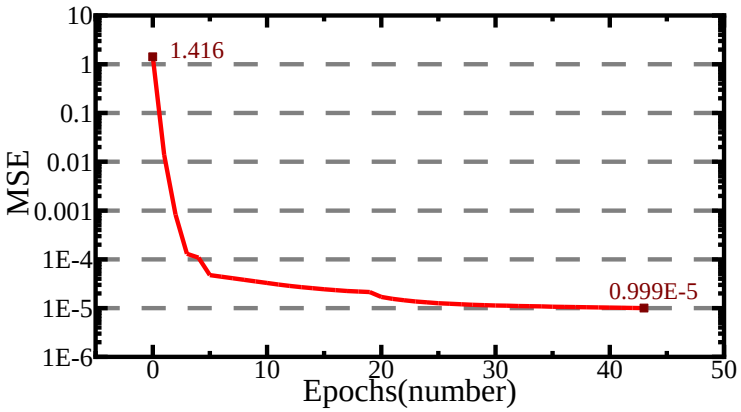

Figure 16. The training process of BPNN

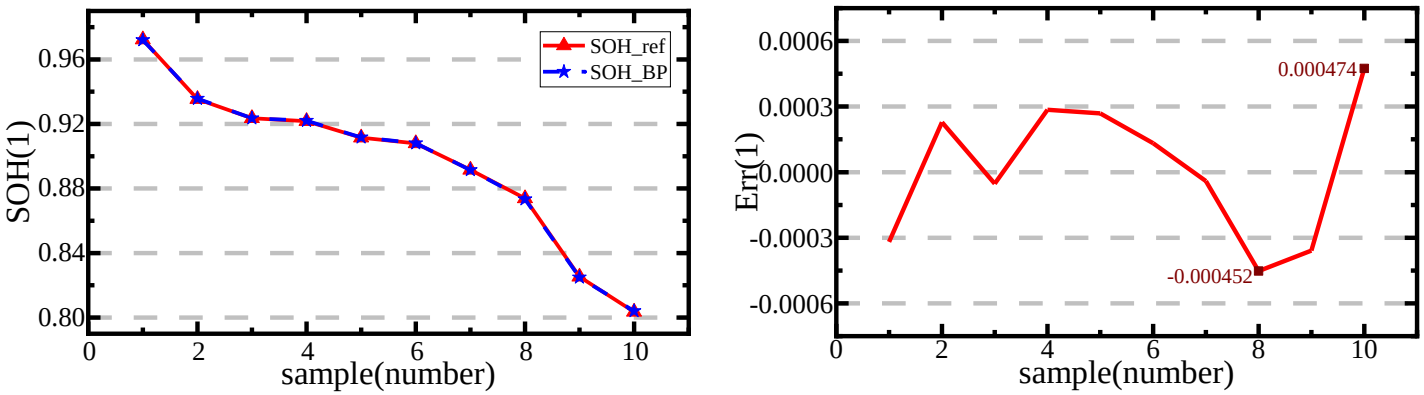

(a) Estimated and actual SOH values (b) The errors of SOH values

Figure 17. SOH values and corresponding errors of 10 sets of samples

It can be seen from Figure 16 that BPNN can meet the set target MSE requirement after 43

repetitions of training. On the basis of recording and storing network connection weights and thresholds, 10 sets of data among 94 sets of data are randomly selected as samples, and 40 times of model training are performed. At this time, the SOH output of the model and the corresponding errors are shown in Figure 17.It can be seen from Figure 17 that the estimation curve basically coincides with the actual curve, which indicates that the BPNN model after training has a good nonlinear mapping ability and can accurately reflect the degradation change of battery capacity. In these 10 sets of samples, the mean absolute error of SOH estimation results is 0.0261%, and the maximum absolute error is 0.0474%. Besides, the MSE of the SOH estimation results is 8.87×10^{-8}. The above results verify the accuracy and superiority of BPNN with $c_{s,max,p}$, $c_{s,max,n}$, LAM and LLI as input.

In order to verify the universality of the BPNN estimation model, another 26650 cell of the same batch was selected for degradation experiments, capacity test experiments and low current discharge experiments at the same temperature and cycle conditions. Besides, in order to obtain the estimated SOH of the second cell during the whole degradation process, it is necessary to use the relevant data of the first cell as the training data and the relevant data of the second cell as the test data. The SOH estimation results of the proposed algorithm and the algorithm using voltage and current as BPNN input are shown in Figure 18(a). The estimation errors of the corresponding algorithms are shown in Figure 18(b).

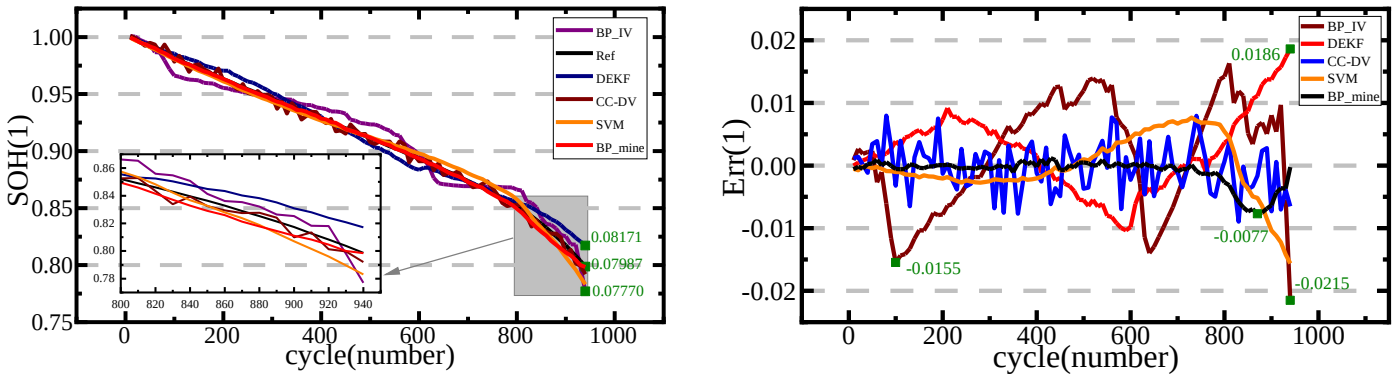

(a) Estimated and actual SOH values (b) The errors of SOH values

Figure 18. Estimated SOH values and the corresponding errors of five algorithms

The results and corresponding errors of the five SOH estimation algorithms are shown in Figure 18. The electrochemical changes of the cells with the same degradation path are similar. In other words, the SP models and the IC-DV curves between cells are similar. Therefore, the model trained by the parameters of a cell can characterize the degradation process of the same batch of cells.

It can be seen from Figure 18(a) that the estimated curve of the BPNN algorithm based on LDW-PSO and IC-DV is basically the same as the actual curve at 25 °C. *Ref* represents the reference value of the SOH. In Figure 18(a), the red line and the black line basically coincide before 800 cycles, which can also be seen in Figure 18(b). Although the tracking accuracy at the end of the curve is reduced, the curve can converge eventually. However, the actual curve and the estimated curve of the BPNN algorithm based on voltage and current[44] have obvious differences in the change trend, and the corresponding errors are also significantly larger. For the dual extended Kalman filtering (DEKF) algorithm[34] and

the SVM[43] method, the errors of SOH estimation results are obviously larger than that of the algorithm proposed in this paper, and the convergence of these two methods is not good. For the coulomb counting-differential voltage (CC-DV) algorithm[41], although the convergence performance of this algorithm is good, the overall estimation errors do not meet the experimental requirements, and its robustness performance is not as good as the algorithm proposed in this paper. The results show that the algorithm based on LDW-PSO and IC-DV has better SOH estimation performance than the other four algorithms and can well simulate the SOH change of the energy storage lithium-ion battery during this degradation process.

The curves in Figure 18(b) show the estimated error values of the above five algorithms. It can be seen from Figure 18(b) that, at 25℃, the maximum error, the mean error and the MSE of the BPNN algorithm based on LDW-PSO and IC-DV are 0.0077, 0.0012 and 5.24×10^{-6}, respectively. On the other hand, at 25°C, the maximum absolute error, the mean absolute error and the MSE of the SOH estimated by the BPNN algorithm based on voltage and current are 0.0215, 0.0078 and 8.06×10^{-5}, respectively, which cannot well meet the engineering requirements of energy storage lithium-ion batteries. The analysis results of these two methods can prove the superiority of the BPNN input parameters proposed in this paper. Besides, at 25°C, the mean absolute errors of DEKF, CC-DV and SVM are 0.0052, 0.0031 and 0.0036, respectively, which show lower performance than the algorithm proposed in this paper. The above results verify the accuracy, superiority and universality of the algorithm proposed in this paper in estimating the SOH of energy storage lithium-ion batteries.

4. CONCLUSIONS

Accurate SOH estimation of energy storage lithium-ion batteries is very important for monitoring and managing battery states in complex working conditions. In this paper, a SP model is established to characterize the electrochemical characteristics of energy storage lithium-ion batteries, and the LDW-PSO algorithm is used to identify a couple of electrochemical parameters. In addition, the quantized values of LAM and LLI are obtained by using the quantification method of degradation modes based on IC-DV. The quantized values and the electrochemical parameters are used as the input of BPNN to estimate the SOH during the battery degradation process. At 25℃, under the working condition of a simulated energy storage power station, the maximum estimation error, the mean estimation error, and the MSE of the battery SOH in test data are 0.0474%, 0.0261%, and 8.87×10^{-8}, respectively. The maximum estimation error, the mean estimation error, and the MSE of the battery SOH in the same batch with the same degradation path are 0.0077, 0.0012, and 5.24×10^{-6}, respectively. The experimental results verify that the algorithm has high accuracy in estimating the SOH of lithium-ion batteries and prove that the algorithm can better meet the estimation requirements of lithium-ion batteries under the condition of energy storage power stations. Compared with the estimation methods based on DEKF, based on CC-DV, and based on SVM developed by other scholars, the algorithm proposed in this paper has obvious advantages. The accurate estimation of SOH is the basis for ensuring the safe and stable operation of the energy storage power station. The algorithm proposed in this paper can effectively avoid the problems caused by the excessive deviation of the battery SOH estimation.

ACKNOWLEDGMENTS
The authors acknowledge the financial support from China Three Gorges Corporation (No. WWKY-2021-0027) and National Key R&D Program of China (2021YFB2400700).

References

1. Y. Jin, Z. Zhao, S. Miao, Q. Wang, L. Sun and H. Lu, *J. Energy Storage*, 42 (2021) 102987.
2. A.G. Olabi, *Energy*, 136 (2017) 1.
3. X. Chen, L. Huang, J. Liu, D. Song and S. Yang, *Energy*, 239 (2022) 121897.
4. F. Gao, H. Liu, K. Yang, C. Zeng, S. Wang, M. Fan and H. Wang, *Int. J. Electrochem. Sci.*, 15 (2020) 1391.
5. R. Zalosh, P. Gandhi and A. Barowy, *J. Loss Prevent. Proc.*, 72 (2021) 104560.
6. G. Jin, L. Li, Y. Xu, M. Hu, C. Fu and D. Qin, *Energies*, 13 (2020) 1785.
7. Z. Chen, L. Yang, X. Zhao, Y. Wang and Z. He, *Appl. Mathe. Modelling*, 70 (2019) 532.
8. J. Li, Q. Lai, L. Wang, C. Lyu and H. Wang, *Energy*, 114 (2016) 1266.
9. Y. Luo, P. Qi, Y. Kan, J. Huang, H. Huang, J. Luo, J. Wang, Y. Wei, R. Xiao and S. Zhao, *Int. J. Energ. Res.*, 44 (2020) 10538.
10. K. Liu, X. Hu, Z. Yang, Y. Xie and S. Feng, *Energ. Convers. Manage.*, 195 (2019) 167.
11. X. Hu, K. Zhang, K. Liu, X. Lin, S. Dey and S. Onori, *IEEE Ind. Electron. Magazine*, 14 (2020) 65.
12. Y. Fan, Y. Bao, C. Lin, Y. Chu, X. Tan and S. Yang, *Appl. Ther. Eng.*, 155 (2019) 96.
13. F. Feng, X. Hu, L. Hu, F. Hu, Y. Li and L. Zhang, *Renew. Sustain. Energ. Rev.*, 112 (2019) 102.
14. R. Xiong, S. Wang, C. Fernandez, C. Yu, Y. Fan, W. Cao and C. Jiang, *Int. J. Electrochem. Sci.*, 16 (2021) 211114.
15. L. Xu, Z. Deng and X. Hu, *IEEE Int. Futr. Energ. Electron. Conf.*, 1 (2021) 1.
16. C. Chang, Y. Zheng and Y. Yu, *Energies*, 13 (2020) 5947.
17. C. Ruhatiya, R. Gandra, P. Kondaiah, K. Manivas, A. Samhith, L. Gao, J. S. Lam and A. Garg, *Int. J. Energ. Res.*, 45 (2020) 6152.
18. Y. Tian, R. Lai, X. Li, L. Xiang and J. Tian, *Appl. Energy*, 265 (2020) 114789.
19. H. Sheng and J. Xiao, *J. Power Sources*, 281 (2015) 131.
20. E. Chemali, P. J. Kollmeyer, M. Preindl and A. Emadi, *J. Power Sources*, 400 (2018) 242.
21. Y. Che, Y. Cai, H. Li, Y. Liu, M. Jiang and P. Qin, *Electrochem. En. Conv. Stor.*, 19 (2022) 021014.
22. Q. Gong, P. Wang and Z. Cheng, *J. Energy Storage*, 46 (2022) 103804.
23. W. Xiong, Y. Mo and C. Yan, *IEEE Access*, 9 (2021) 1.
24. Y. Zhang, Y. Liu, J. Wang and T. Zhang, *Energy*, 239 (2022) 121986.
25. J. Li, M. Ye, K. Gao, X. Xu, M. Wei and S. Jiao, *Int. J. Energ. Res.*, 45 (2021) 13307.
26. J. Qiao, S. Wang, C. Yu, W. Shi and C. Fernandez, *Int. J. Circ. Theor. Appl.*, 49 (2021) 3879.
27. M. Zeng, P. Zhang, Y. Yang, C. Xie and Y. Shi, *Energies*, 12 (2019) 3122.
28. L. Ling and Y. Wei, *IEEE Access*, 9 (2021) 2169.
29. M. Doyle, T. F. Fuller and J. Newman, *J. Electrochem. Soc.*, 140 (2019) 1526.
30. L. Ren, G. Zhu, J. Kang, J. Wang, B. Luo, C. Chen and K. Xiang, *J. Energy Storage*, 39 (2021) 102644.
31. R. Mehta and A. Gupta, *Electrochim. Acta*, 389 (2021) 138623.
32. Z. Deng, L. Yang, H. Deng, Y. Cai and D. Li, *Energy*, 142 (2018) 838.
33. M.J. Esfandyari, M.R. Hairi Yazdi, V. Esfahanian, M. Masih-Tehrani, H. Nehzati and O. Shekoofa, *J. Energy Storage*, 24 (2019) 100758.
34. J. Park, M. Lee, G. Kim, S. Park and J. Kim, *Energies*, 13 (2020) 2138.

35. Z. Chu, G.L. Plett, M.S. Trimboli and M. Ouyang, *J. Energy Storage*, 25 (2019) 100828.
36. V. Ramadesigan, P.W.C. Northrop and S. De, *J. Electrochem. Soc.*, 159 (2012) 31.
37. S.E. Li, B. Wang, H. Peng and X. Hu, *J. Power Sources*, 258 (2014) 9.
38. C. Fernandez, K. Uddin, G.H. Chouchelamane, W.D. Widanage and J. Marco, *J. Power Sources*, 360 (2017) 301.
39. D. Ansean, V.M. Garcia, M. Gonzalez, C. Blanco-Viejo, J.C. Viera, Y.F Pulido and L. Sanchez, *IEEE Trans. Ind. Appl.*, 55 (2019) 2992.
40. M. Lewerenz, A. Marongiu, A. Warnecke and D.U. Sauer, *J. Power Sources*, 368 (2017) 57.
41. S. Zhang, X. Guo, X. Dou and X. Zhang, *J. Power Sources*, 479 (2020) 228740.
42. K.K. Sadabadi, X. Jin and G. Rizzoni, *J. Power Sources*, 481 (2021) 228861.
43. X. Tan, D. Zhan, P. Lyu, J. Rao and Y. Fan, *J. Power Sources*, 484 (2021) 229233.
44. D. Yang, Y. Wang, R. Pan, R. Chen and Z. Chen, *Energy Procedia*, 105 (2017) 2059.